RSC Advances

PAPER

View Article Online
View Journal | View Issue

Cite this: *RSC Adv.*, 2026, **16**, 25912

Adjunctive therapeutic strategy for in-stent thrombosis: *in vitro* pharmacodynamic evaluation of COX-1 inhibitor 3d combined with catheter-directed thrombolysis

Bo Ma, * Zenghui Liang, Liping Fu, Yanbiao Ma, Qinghe Sun and Xuchen Lv

Twelve benzohydrazide Schiff base derivatives (**3a–3l**) with systematic variations in the aromatic aldehyde moiety were designed and synthesized to evaluate their anti-inflammatory, antiplatelet, and *in vitro* antithrombotic activities. Among them, compound **3d** (the condensation product of 4-chlorobenzohydrazide and furan-2-carbaldehyde) was identified as the most promising lead, displaying moderately selective COX-1 inhibition (IC_{50} = 1.63 μM, selectivity index = 8.87) together with moderate 5-LOX inhibition (IC_{50} = 10.63 μM). In LPS-stimulated macrophages, **3d** concentration-dependently suppressed the release of TNF-α, IL-6, IL-1β, and PGE_2. It inhibited ADP- and collagen-induced platelet aggregation (IC_{50} = 5.48 μM and 4.52 μM, respectively), reduced the expression of platelet activation markers CD62P and PAC-1, and prolonged clotting time while decreasing clot strength in thromboelastography. Under arterial shear conditions in a parallel-plate flow chamber, **3d** significantly attenuated thrombus formation in a concentration-dependent manner. Importantly, in an *in vitro* clot lysis model, **3d** (50 μM) enhanced the thrombolytic rate of low-dose urokinase (100 IU per mL) from 35.0% to 45.2%, highlighting its potential to augment thrombolysis. Preliminary ADME profiling revealed moderate plasma protein binding (89.3%) and a metabolic half-life of 0.75 h in liver microsomes. This study provides the first systematic structure–activity relationship analysis of aromatic aldehyde substituents on benzohydrazide Schiff bases and identifies **3d** as a lead compound possessing combined anti-inflammatory, antiplatelet, and thrombolysis-enhancing activities. These findings support the potential of **3d** as an adjunctive agent for catheter-directed thrombolysis in in-stent thrombosis, pending further *in vivo* efficacy and safety investigations.

Received 4th March 2026
Accepted 2nd May 2026

DOI: 10.1039/d6ra01870j

rsc.li/rsc-advances

1. Introduction

Venous thromboembolism (VTE), a collective term for deep vein thrombosis and pulmonary embolism, is the third most common cause of cardiovascular disease-related death after myocardial infarction and stroke. It poses a serious threat to human health, with its incidence increasing significantly, particularly in the elderly population.[1,2] Currently, the standard treatment for VTE primarily relies on anticoagulant drugs (such as direct oral anticoagulants, warfarin, and heparin) as well as mechanical interventions like thrombolysis or surgical thrombectomy.[3] However, these traditional therapies have significant limitations: anticoagulant therapy multiplies the risk of major bleeding and has numerous contraindications; simultaneously, existing methods are limited in their ability to promote spontaneous thrombus dissolution and prevent thrombus recurrence.[4–6] Therefore, there is an urgent clinical need for the development of novel therapeutic agents with novel mechanisms of action, improved safety profiles, and the capacity to effectively intervene throughout the entire process of thrombus formation.

In recent years, advances in basic research have provided the academic community with a new understanding of the pathogenesis of VTE. The concept of "thromboinflammation" has been proposed, revealing a complex and intricate "bidirectional crosstalk" between inflammation and the coagulation system.[7] On one hand, inflammatory responses can activate the coagulation system: activated inflammatory cells and damaged endothelial cells highly express tissue factor, initiating the extrinsic coagulation cascade; simultaneously, inflammatory mediators such as tumor necrosis factor-α (TNF-α) and interleukin-1β (IL-1β) can downregulate the function of natural anticoagulant pathways, collectively creating a hypercoagulable state.[8,9] On the other hand, activation of the coagulation system can, in turn, exacerbate inflammatory responses: activated coagulation factors and platelets not only directly participate in thrombus formation but can also induce endothelial cells and

Cangzhou People's Hospital, Interventional Vascular Surgery, Cangzhou, 061000, China. E-mail: bobo73112026@163.com

monocytes to express adhesion molecules and pro-inflammatory cytokines by activating protease-activated receptors, forming a vicious cycle.[10,11]

Within this thromboinflammatory network, macrophages play a central and multifaceted role. Upon exposure to pro-inflammatory stimuli such as lipopolysaccharide (LPS), macrophages undergo classical activation and produce large amounts of TNF-α, IL-6, IL-1β, and tissue factor, thereby promoting both local inflammation and a procoagulant state.[12] Recent studies have further highlighted that macrophage-derived cytokines can directly enhance platelet reactivity and amplify the thromboinflammatory response.[13] In the context of in-stent thrombosis and arterial thromboinflammation, infiltrating macrophages accumulate at the site of vascular injury or stent struts, where they perpetuate chronic inflammation, contribute to neointimal hyperplasia, and destabilize the thrombus.[14] Therefore, an *in vitro* model using LPS-stimulated RAW264.7 macrophages is widely accepted as a relevant and reproducible system to evaluate the anti-inflammatory potential of novel compounds, as it recapitulates key aspects of macrophage activation and allows quantitative assessment of pro-inflammatory cytokine release.[15]

The discovery of the thromboinflammation network has pointed the way towards therapeutic targets beyond traditional anticoagulation—by targeting inflammatory pathways, it may be possible to effectively inhibit thrombosis without increasing the risk of bleeding. Within the interactive network of inflammation and thrombosis, cyclooxygenase (COX) and platelets serve as key nodes connecting the two systems.[16] COX is the crucial rate-limiting enzyme in the metabolism of arachidonic acid to prostaglandins and exists as two main isoenzymes: constitutively expressed COX-1 and inducibly expressed COX-2.[17] In the context of thromboinflammation, their roles have distinct emphases. COX-1 occupies a central position in regulating platelet function; its metabolite, thromboxane A_2, is a potent mediator that induces platelet aggregation and vasoconstriction. Selective inhibition of COX-1 is a classic antiplatelet therapeutic strategy.[18,19] On the other hand, COX-2 is a core enzyme in inflammatory responses, with its expression upregulated upon stimulation by LPS, cytokines, *etc.*, producing large amounts of pro-inflammatory prostaglandin E_2 (PGE_2) that drive local and systemic inflammation.[20] Furthermore, activated platelets are not only the "building material" of thrombi but also crucial regulators of inflammatory responses. Upon platelet activation, *P*-selectin (CD62P) is rapidly expressed on their surface, mediating the formation of platelet-leukocyte aggregates through binding to *P*-selectin glycoprotein ligand-1 on leukocytes. This is a key event directly linking inflammation and thrombosis.[21] Concurrently, activated platelets can also release various pro-inflammatory mediators such as CD40 ligand and IL-1β, exacerbating vascular inflammation.[22] Emerging evidence has revealed novel platelet activation pathways involving oxidative stress and specific signaling cascades that are potential targets for antiplatelet therapy.[23,24] Moreover, recent studies have explored the molecular mechanisms of atherosclerosis-related inflammation, showing that targeting specific inflammatory mediators can reduce both plaque progression and thrombotic complications.[25] In parallel with advances in understanding thromboinflammation, novel thrombolytic strategies are being developed to improve the efficacy and safety of catheter-directed thrombolysis. Recent studies have explored the use of nano-formulated thrombolytics, combination therapy with antiplatelet agents, and targeted fibrinolytic approaches to reduce the required dose of plasminogen activators and minimize bleeding complications.[26,27] These strategies underscore the clinical need for adjunctive agents that can enhance thrombus dissolution while maintaining a favorable safety profile.

Schiff bases, characterized by the imine group (–C═N–), are privileged scaffolds in medicinal chemistry due to their synthetic accessibility and diverse biological activities.[28] Research has shown that Schiff bases and their metal complexes exhibit promising anti-inflammatory, antioxidant, antibacterial, and even antitumor activities.[29,30] In the field of anti-inflammation, studies have confirmed that specific Schiff base analogs can act as selective COX-1 inhibitors, effectively inhibiting platelet aggregation induced by ADP and collagen.[31] Previous reports have demonstrated that benzohydrazide derivatives bearing heteroaromatic rings exhibit potent antiplatelet and anti-inflammatory activities, but a systematic comparison of different aromatic aldehyde substituents – including benzoic acid, phenol, biphenyl, furan, thiophene and pyridine – on the combined anti-inflammatory, antiplatelet and hemocompatibility profiles of benzohydrazide-based Schiff bases has been lacking.[32]

Based on this, we designed twelve Schiff base derivatives (**3a**–**3l**) with systematic variations in the benzohydrazide core (methyl/chloro) and aromatic aldehydes (benzoic acid, phenol, biphenyl, furan, thiophene, pyridine). Their anti-inflammatory, antiplatelet, and antithrombotic activities were evaluated *in vitro*, and lead compound **3d** was tested in a thrombolysis synergy model mimicking catheter-directed thrombolysis. The findings are expected to provide lead compounds for novel anti-inflammatory and antithrombotic drugs.

2. Results and discussion

2.1 Chemical synthesis

Several previous studies have reported the anti-inflammatory and antiplatelet activities of Schiff base and benzohydrazide derivatives. For example, Lamie and co-workers synthesized a series of *N*-substituted indole Schiff bases that acted as dual COX-2/5-LOX inhibitors, demonstrating that the Schiff base scaffold can effectively modulate arachidonic acid metabolism.[31] A comprehensive review by Khan *et al.* highlighted that heterocyclic Schiff bases bearing furan, thiophene, or pyridine rings often exhibit improved lipophilicity and enhanced binding affinity to cyclooxygenase enzymes, making them promising leads for anti-inflammatory and antiplatelet drug development.[28] Further research has extended the scope of antithrombotic strategies to include immune modulation approaches that may attenuate in-stent restenosis,[33] while continued structural optimization of Schiff base derivatives has yielded compounds with dual COX-2/5-LOX inhibitory activity.[34]

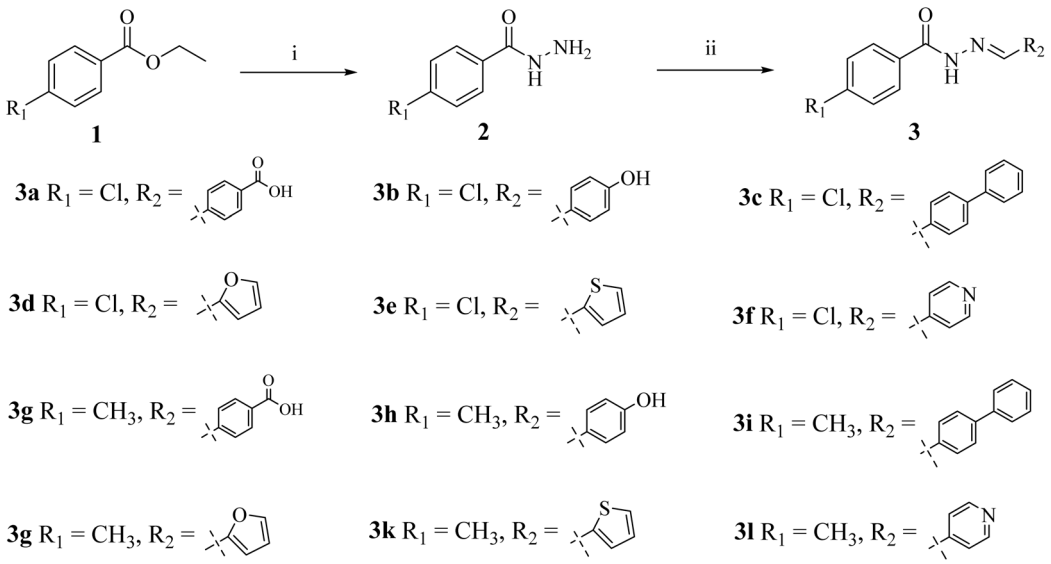

Fig. 1 Synthesis of Schiff base derivatives **3a–3l**. Conditions and reagents: (i) ethanol, $NH_2NH_2 \cdot H_2O$, reflux, 6–8 h, yield 86%; (ii) ethanol, *R*–CHO, reflux, 4–6 h, yield 81–93%.

A systematic comparison of structurally diverse aromatic aldehydes (including benzoic acid, phenol, biphenyl, furan, thiophene, and pyridine) combined with methyl or chloro substituents on the benzohydrazide core has not been performed. Furthermore, the hemocompatibility and the potential to enhance thrombolysis of such derivatives have rarely been explored.

Based on this, in the present study, twelve Schiff base derivatives (compounds **3a–3l**) were synthesized from ethyl *p*-methylbenzoate and ethyl *p*-chlorobenzoate as starting materials *via* a two-step reaction following previously reported methods (Fig. 1).[35,36] First, the starting materials underwent hydrazinolysis with hydrazine hydrate to yield the key intermediates, 4-methylbenzohydrazide and 4-chlorobenzohydrazide, respectively. Subsequently, these intermediates were subjected to Schiff base condensation reactions with six structurally diverse aromatic aldehydes (4-formylbenzoic acid, 4-hydroxybenzaldehyde, 4-biphenylcarboxaldehyde, furan-2-carbaldehyde, thiophene-2-carbaldehyde, and pyridine-4-carbaldehyde), successfully affording the twelve target compounds in yields ranging from 81% to 93%. The structures of all target compounds were comprehensively confirmed by proton nuclear magnetic resonance (^{1}H NMR), carbon-13 nuclear magnetic resonance (^{13}C NMR), and high-resolution mass spectrometry (HR-MS), with the spectral data consistent with the expected structures. In the ^{1}H NMR spectra, all compounds exhibited a singlet signal for the N–H proton of the hydrazide group within the range of δ 11.90–11.50 ppm and a characteristic singlet signal for the imine (–N=CH–) proton within the range of δ 8.60–8.40 ppm. Aromatic proton signals were distributed in the δ 7.98–6.60 ppm region, with integrations consistent with the number of aromatic protons in each compound's structure. In the ^{13}C NMR spectra, all compounds displayed a signal for the amide carbonyl carbon in the range of δ 165.0–163.0 ppm and a signal for the imine carbon (C=N) in the range of δ 150.0–148.0 ppm, further confirming the target structures. The purity of the compounds was analyzed using high-performance liquid chromatography (HPLC), and the results showed that all compounds had a purity greater than 95%, meeting the requirements for subsequent biological activity testing.

2.2 Cellular safety evaluation of compounds

The cytotoxicity of the twelve compounds (**3a–3l**) against RAW264.7 mouse macrophages was evaluated using the MTT assay.[37] Cell viability was determined after treatment with various concentrations (5, 25, 50, 100, 200 μM) of the compounds for 24 hours. The results showed that within the concentration range of 5–100 μM, cell viability for all compound-treated groups was above 90%, showing no significant difference compared to the solvent control group (0.1% DMSO). When the concentration was increased to 200 μM, some compounds (**3a**, **3c**, **3f**, **3l**) exhibited slight cytotoxicity, with cell viability decreasing to between 70–85%, while the remaining compounds still maintained cell viability above 85% at this concentration (Fig. 2A).

The erythrocyte hemolysis assay was further employed to assess the membrane-damaging effects of the target compounds on red blood cells, thereby evaluating their hemocompatibility.[38] Human red blood cell suspensions were incubated with the compounds at concentrations of 25, 50, and 100 μM, and the hemolysis rates were measured. The results indicated that within the 25–50 μM concentration range, the hemolysis rates for all tested compounds were below 2%, showing no significant difference compared to the negative control group (0.1% DMSO). This suggests that the compounds do not cause significant hemolysis within this concentration range. When the concentration was increased to 100 μM

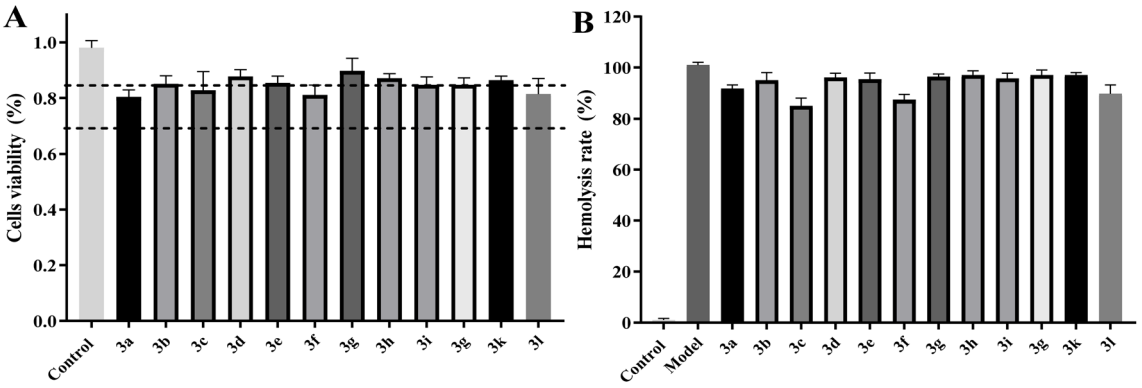

Fig. 2 (A) Viability rates of RAW264.7 cells treated with compounds (200 μM) after 24 h. (B) Hemolysis rates of compounds on human red blood cells. Human red blood cells were incubated with the compounds (100 μM) at 37 °C. 0.1% DMSO and 1% Triton X-100 were used as negative and positive controls, respectively.

(Fig. 2B), the hemolysis rates for some compounds (*e.g.*, **3a**, **3c**, **3f**, **3l**) slightly increased to between 5–15%; for the remaining compounds, hemolysis rates remained below 5% at this concentration. The positive control, Triton X-100 (1%), induced complete hemolysis.

2.3 Selective inhibitory activities of compounds against COX-1/COX-2

The *in vitro* inhibitory activities of the twelve compounds against COX-1, COX-2, and 5-LOX were determined using enzyme activity assay kits,[39] and the results are summarized in Table 1. The IC_{50} values of all compounds against COX-1 ranged from 1.63 to 15.71 μM, against COX-2 from 11.38 to 21.36 μM, and against 5-LOX from 10.63 to 26.43 μM. The active compound **3d** exhibited the most potent inhibitory activity against COX-1 (IC_{50} = 1.63 μM). Meanwhile, **3d** showed relatively weaker inhibitory activity against COX-2 (IC_{50} = 14.47 μM) and moderate inhibitory activity against 5-LOX (IC_{50} = 10.63 μM). The calculated COX-1 selectivity index (SI = COX-2 IC_{50}/COX-1 IC_{50}) was 8.87, indicating that **3d** possesses high selectivity for COX-1 and has the potential to regulate the dual-pathway metabolism of arachidonic acid. Considering the compounds' high selective inhibitory activity against COX-1 (SI value) and their inhibitory effects on 5-LOX, we selected the most representative moderately selective COX-1 inhibitor **3d** and **3e**, which possesses good dual COX-1/5-LOX inhibitory activity, for subsequent validation of anti-inflammatory activity at the cellular level.

Table 1 Inhibitory activities of compounds against COX-1, COX-2, and 5-LOX (IC_{50}, μM)

Compound	COX-1 IC_{50}	COX-2 IC_{50}	5-LOX IC_{50}	SI
3a	14.82 ± 0.35	15.24 ± 1.21	24.36 ± 1.18	1.03
3b	12.13 ± 0.18	19.58 ± 0.76	21.24 ± 0.95	1.61
3c	8.47 ± 0.62	21.36 ± 1.87	22.65 ± 1.84	2.52
3d	1.63 ± 0.08	14.47 ± 0.92	10.63 ± 0.71	8.87
3e	1.95 ± 0.09	11.38 ± 0.98	11.42 ± 0.78	5.84
3f	8.26 ± 0.24	12.43 ± 1.05	25.38 ± 1.26	1.50
3g	7.23 ± 0.56	18.46 ± 1.54	19.27 ± 1.58	2.55
3h	13.84 ± 0.29	13.67 ± 1.08	26.43 ± 1.35	0.99
3i	8.26 ± 0.58	19.52 ± 1.63	21.58 ± 1.72	2.36
3j	11.42 ± 0.11	19.15 ± 0.78	20.26 ± 0.84	1.68
3k	12.13 ± 0.15	11.84 ± 0.95	22.57 ± 1.02	0.98
3l	15.71 ± 0.43	14.25 ± 1.16	17.34 ± 1.42	0.91
Celecoxib	12.8 ± 1.02	0.06 ± 0.01	—	0.0047
Ibuprofen	13 ± 0.92	370 ± 4.32	—	28
Zileuton	—	—	7.25 ± 0.61	—

2.4 Inhibitory effects of compounds on LPS-induced inflammatory response in macrophages

Based on the enzyme activity screening results, two representative compounds (**3d** and **3e**) were selected for validation of anti-inflammatory activity at the cellular level. An inflammation model was established by stimulating RAW264.7 macrophages with LPS (1 μg mL^{-1}), and the effects of the compounds on the release of inflammatory factors TNF-α, IL-6, IL-1β, and PGE_2 were detected using ELISA.[40] The results showed (Fig. 3) that after LPS stimulation, the levels of TNF-α, IL-6, IL-1β, and PGE_2 in the model group were significantly increased compared to the blank control group. All tested compounds inhibited the LPS-induced release of inflammatory factors in a concentration-dependent manner. Among them, the target compound **3d** exhibited stronger inhibitory effects: at a concentration of 50 μM, the inhibition rates for IL-6, TNF-α, IL-1β, and PGE_2 were 37.8%, 41.8%, 51.7%, and 54.6%, respectively. Compound **3e** also showed good anti-inflammatory activity, but its inhibition rates were lower than those of **3d** at the same concentration. These results indicate that compound **3d** can effectively inhibit the inflammatory cascade triggered by LPS at the cellular level, which is consistent with its selective COX-1 inhibitory activity.

2.5 Inhibitory effects of compounds on platelet function and whole blood thrombus formation

2.5.1 Inhibitory effect on platelet aggregation. The inhibitory effect of the preferred compound **3d** on human platelet aggregation was evaluated using the turbidimetric method, with aspirin as a positive control.[41] Aggregation was induced by

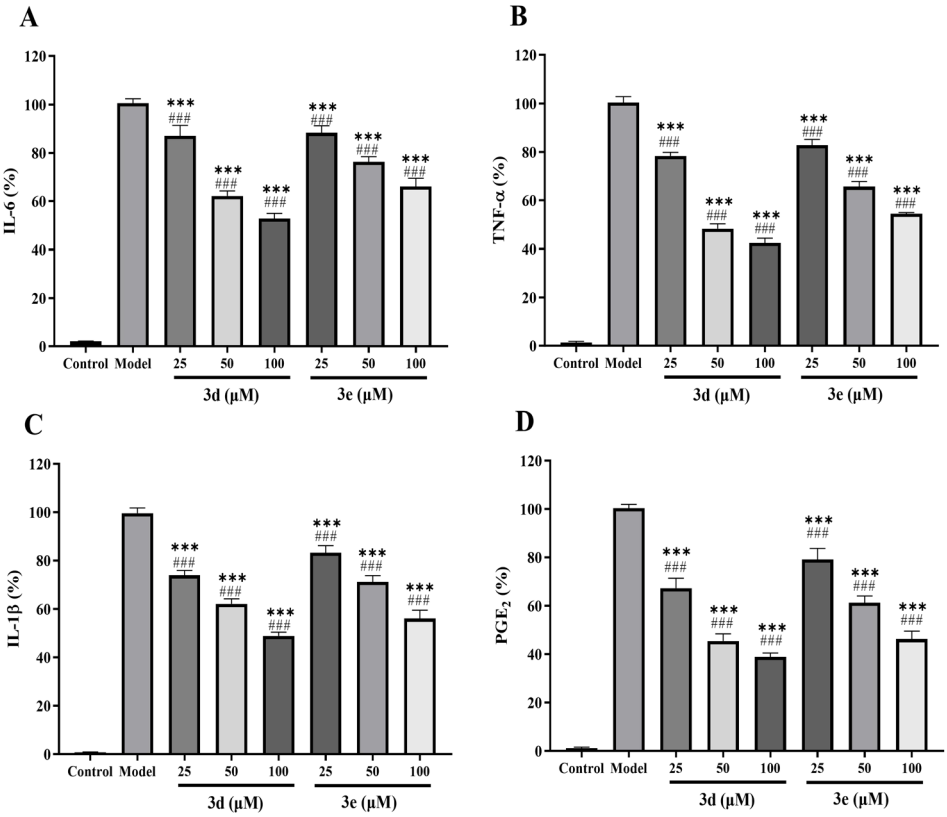

Fig. 3 The anti-inflammatory activities of compounds **3d** and **3e** were assessed in LPS-induced RAW264.7 macrophages by ELISA. (A) **3d** and **3e** affects the level of IL-6. (B) **3d** and **3e** affects the level of TNF-α. (C) **3d** and **3e** affects the level of IL-1β. (D) **3d** and **3e** affects the level of PGE_2. Compared with the LPS model group, $^{*}p < 0.05$, $^{**}p < 0.01$, $^{***}p < 0.001$; $^{\#\#\#}p < 0.001$ *vs.* control group. Data are presented as means ± SEM from three independent experiments.

Table 2 Inhibitory effects of compounds on human platelet aggregation induced by ADP, collagen, and arachidonic acid (IC_{50}, μM)

Compound	Inducer: ADP	Inducer: collagen	Inducer: AA
3d	5.48 ± 0.03	4.52 ± 0.04	2.92 ± 0.45
3e	9.57 ± 0.04	11.66 ± 0.05	6.36 ± 0.43
Aspirin	4.49 ± 0.04	3.51 ± 0.04	2.81 ± 0.16

ADP (10 μM), collagen (2 μg mL^{-1}), or arachidonic acid (AA, 1 mM). As summarized in Table 2, compound **3d** exhibited potent inhibitory activity against AA-induced aggregation with an IC_{50} of 2.92 μM, which is consistent with its COX-1 enzyme inhibitory activity (IC_{50} = 1.63 μM, Table 1). Compound **3d** also inhibited ADP- and collagen-induced aggregation with IC_{50} values of 5.48 μM and 4.52 μM, respectively. Under the same experimental conditions, the positive control aspirin showed IC_{50} values of 2.81 μM (AA), 3.51 μM (collagen), and 4.49 μM (ADP). The rank order of potency (AA > collagen > ADP) for both **3d** and aspirin is consistent with their mechanism as COX-1 inhibitors, as AA-induced aggregation is entirely dependent on the COX-1/TXA_2 pathway, while collagen and ADP also engage additional signaling pathways.

It is worth noting that although compound **3d** and aspirin both inhibit COX-1, their pharmacological mechanisms differ. Aspirin irreversibly acetylates Ser530 in the COX-1 active site, leading to permanent enzyme inactivation for the lifespan of the platelet.[42] In contrast, compound **3d** acts as a competitive and reversible inhibitor (Section 2.6, K_i = 2.8 μM). This difference may have clinical implications: a reversible inhibitor could allow faster recovery of platelet function after drug withdrawal, potentially reducing bleeding risk, whereas aspirin's irreversible action provides sustained antiplatelet effect but increases bleeding tendency. The similar IC_{50} values of **3d** and aspirin in AA-induced aggregation (2.92 μM *vs.* 2.81 μM) reflect their comparable potency at the enzyme level, but the reversibility of **3d** may offer a safety advantage in adjunctive catheter-directed thrombolysis, where rapid reversal of antiplatelet effect might be desirable in case of bleeding complications.

2.5.2 Effect on platelet activation markers. The effect of compound **3d** on platelet activation markers *P*-selectin (CD62P) and PAC-1 binding was detected using flow cytometry.[43] As shown in Fig. 4, under resting conditions, both the CD62P positivity rate and PAC-1 binding rate on the platelet surface were below 5%. After ADP stimulation, the CD62P positivity rate in the model group increased to 63.8%, and the PAC-1 positivity rate increased to 60.1%, indicating significant platelet activation. Compound **3d** concentration-dependently inhibited ADP-induced CD62P expression and PAC-1 binding: at a concentration of 50 μM, the CD62P positivity rate decreased to 32.1%

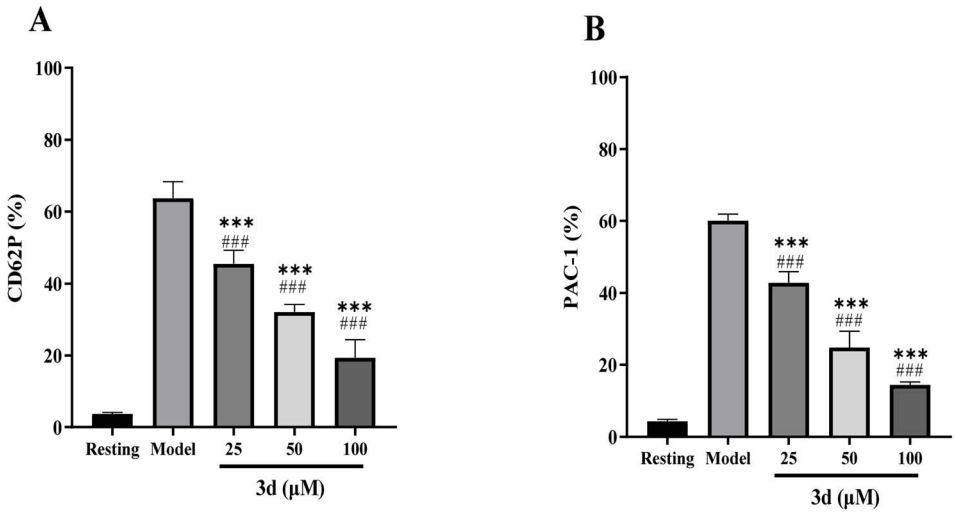

Fig. 4 Effect of compound **3d** on ADP-induced platelet activation marker expression. (A) CD62P positivity rate; (B) PAC-1 binding rate. Platelet-rich plasma was pre-incubated with different concentrations of compound **3d** for 15 min, then activated by adding ADP (10 μM), and the expression of CD62P and PAC-1 on the platelet surface was detected. Compared with model group, $^{*}p < 0.05$, $^{**}p < 0.01$, $^{***}p < 0.001$; $^{\#\#\#}p < 0.001$ *vs.* control group. Data are presented as means ± SEM from three independent experiments.

(inhibition rate of 49.7%), and the PAC-1 positivity rate decreased to 24.8% (inhibition rate of 58.7%). These results indicate that **3d** can not only inhibit platelet aggregation but also effectively inhibit platelet α-granule release and glycoprotein IIb/IIIa receptor activation.

2.5.3 Effect on whole blood thrombus formation. The effect of compound **3d** on the coagulation process of healthy human whole blood was detected using a thromboelastography analyzer,[44] and the results are shown in Fig. 5. Compared with the control group, compound **3d** prolonged the reaction time (*R* time) in a concentration-dependent manner: at concentrations of 25, 50, and 100 μM, the *R* time was extended to 7.2, 9.0, and 11.4 min, respectively. Meanwhile, the maximum amplitude (MA value) gradually decreased from 62.3 mm in the control group to 58.1, 51.1, and 45.0 mm, indicating a reduction in the maximum strength of the blood clot, which was consistent with its inhibitory effect on platelet aggregation. Additionally, the *K* time was prolonged with increasing concentrations, and the *α* angle correspondingly decreased, further confirming that compound **3d** can simultaneously affect coagulation factor function and platelet function in the whole blood system. These results indicate that compound **3d** exerts a moderate *in vitro* antithrombotic effect in the whole blood system containing red blood cells, white blood cells, platelets, and all coagulation factors.

2.5.4 Parallel-plate flow chamber assay for thrombus formation under arterial shear. To evaluate the antithrombotic activity of compound **3d** under arterial flow, human whole blood was perfused over a collagen-coated surface at 1000 s^{-1} for 5 min in a parallel-plate flow chamber, with or without **3d** (25, 50, 100 μM).[45] Thrombus formation was quantified by BCA protein assay, and platelet coverage was analyzed by bright-field microscopy using ImageJ. As shown in Fig. 6A and B, control blood formed robust thrombi with a total protein content of 45.0 μg per chamber and a platelet coverage of 75.1%. Compound **3d** reduced both parameters in a concentration-dependent manner. At 25 μM, thrombus protein decreased to 38.3 μg (14.8% inhibition, $p < 0.01$), and platelet coverage dropped to 58.3%. At 50 μM, protein content was 25.3 (43.8% inhibition, $p < 0.001$) and coverage was 45.2%. At the highest concentration (100 μM), thrombus protein fell to 16.1 μg (64.2% inhibition, $p < 0.001$) and coverage to 24.1%. These results demonstrate that compound **3d** effectively inhibits platelet thrombus formation under arterial shear conditions, providing direct *in vitro* evidence of its flow-dependent antithrombotic potential.

2.5.5 Synergistic effect of compound 3d on urokinase thrombolysis and its clinical significance. In-stent thrombosis is a serious complication following lower extremity arterial intervention. Although catheter-directed thrombolysis is commonly used in clinical practice and is effective, it still has limitations such as high urokinase dosage, prolonged thrombolysis time, and increased bleeding risk.[46,47] Previous experiments have confirmed that compound **3d** possesses good antiplatelet aggregation and platelet activation inhibitory activities. Based on this, this study further investigated whether compound **3d** could enhance the thrombolytic effect of urokinase, providing experimental evidence for its potential as an adjunctive agent for catheter-directed thrombolysis.

An *in vitro* thrombus dissolution experiment was employed to evaluate the synergistic effect of compound **3d** and urokinase. Human platelet-rich plasma was incubated with thrombin and $CaCl_2$ in 96-well plates to form stable platelet-rich thrombi. After weighing the initial thrombus weight, different treatments were added: control group (saline), low-dose urokinase group (100 IU per mL), high-dose urokinase group (500 IU per mL), **3d** monotherapy group (50 μM), low-dose combination group (100 IU per mL urokinase + 50 μM **3d**), and high-dose combination

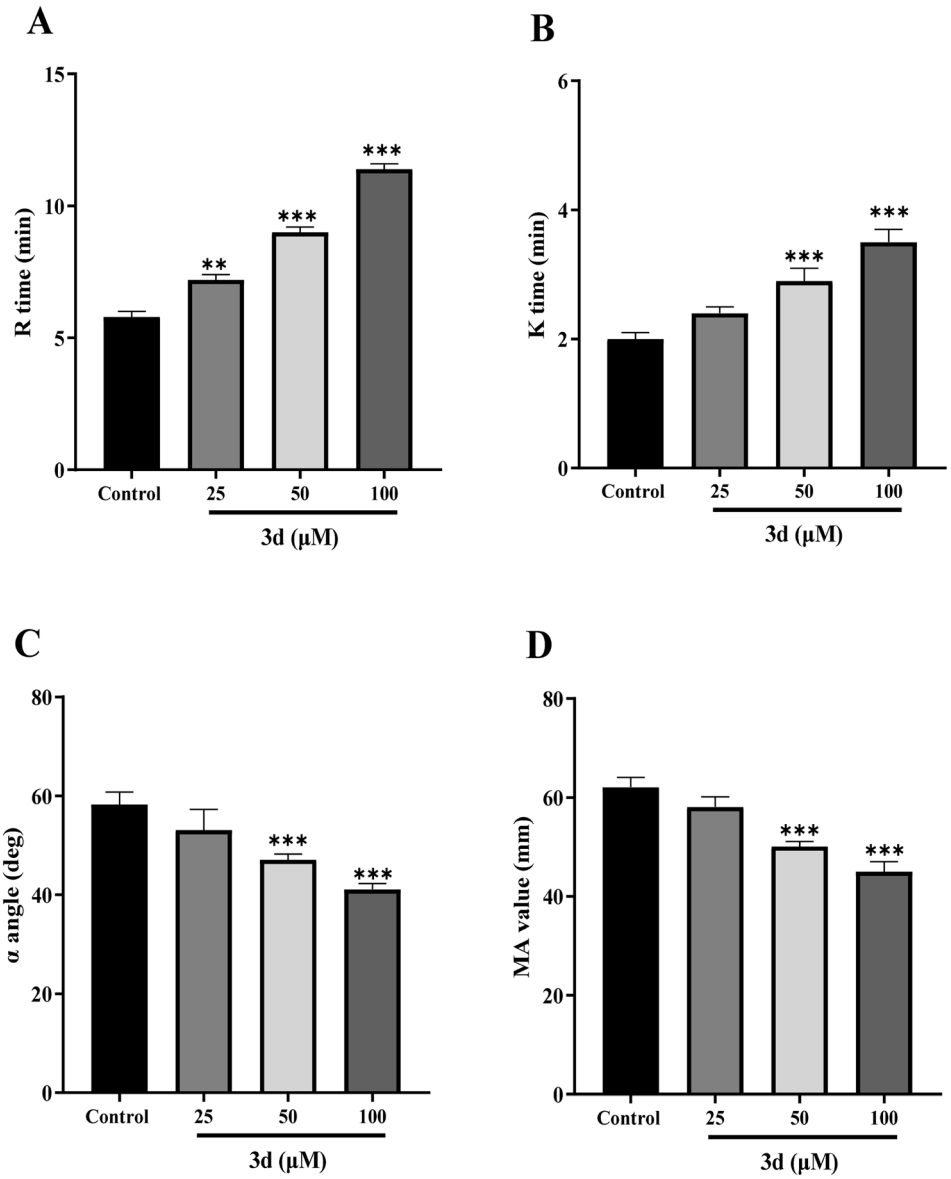

Fig. 5 Healthy human whole blood was incubated with different concentrations of compound **3d** (25, 50, 100 μM), and coagulation parameters were measured using thromboelastography. (A) Reaction time (*R* time); (B) clotting time (*K* time); (C) *α* angle; (D) maximum amplitude (MA value). Data are presented as mean ± SD from three independent experiments. Compared with the control group, **p* < 0.05, ***p* < 0.01, ****p* < 0.001.

group (500 IU per mL urokinase + 50 μM **3d**). After incubation at 37 °C for 2 hours, the remaining thrombus weight was measured to calculate the thrombolysis rate; simultaneously, the supernatant was collected to detect D-dimer levels. The results are shown in Fig. 7. **3d** alone caused only slight thrombus dissolution (thrombolysis rate of 11.3%). Urokinase induced thrombus dissolution in a concentration-dependent manner, with thrombolysis rates of 35.0% in the low-dose group and 60.3% in the high-dose group. Notably, the thrombolysis rate in the low-dose combination group (100 IU per mL urokinase + **3d**) was significantly increased to 45.2%. The D-dimer detection results were consistent with the trend in thrombolysis rates, with significantly enhanced fibrinolytic activity in the combination groups.

These results indicate that compound **3d** can significantly enhance the *in vitro* thrombolytic effect of urokinase, maintaining equivalent thrombolytic efficiency while reducing the urokinase dosage. This synergistic effect may stem from the inhibition of platelet activation by **3d**: by blocking COX-1-mediated thromboxane A_2 generation, **3d** inhibits platelet aggregation and *α*-granule release, resulting in a looser thrombus structure that increases urokinase penetration and contact with fibrin, thereby improving thrombolytic efficiency. In the clinical context, in-stent thrombi are rich in activated platelets, making it difficult for thrombolytic drugs alone to rapidly penetrate and dissolve the thrombus. Combining with antiplatelet agents may overcome this bottleneck. Therefore, compound **3d** has potential as an adjunctive agent for catheter-

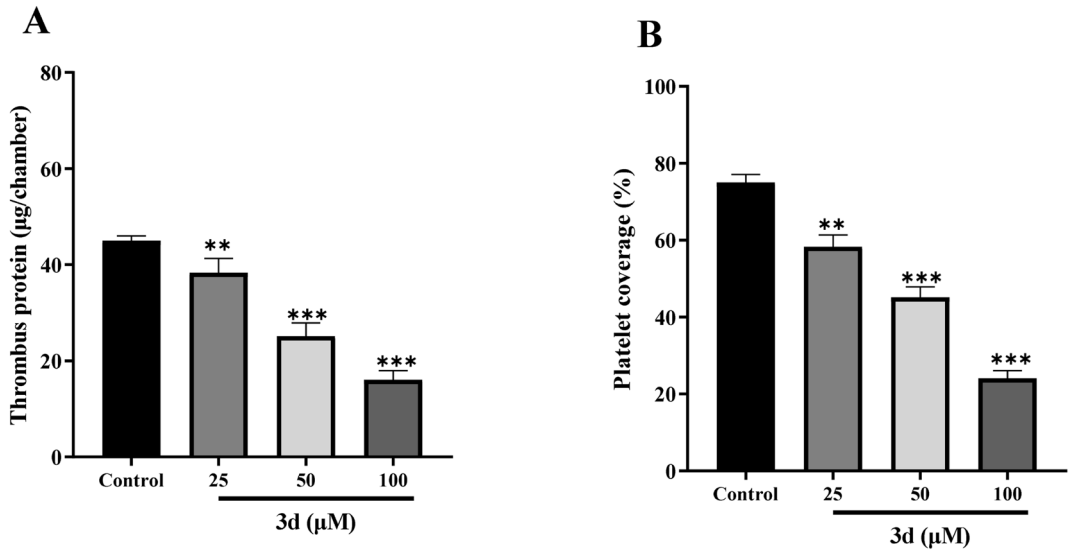

Fig. 6 Antithrombotic activity of compound **3d** under arterial flow in a parallel-plate flow chamber. (A) Thrombus protein content measured by BCA assay. (B) Platelet coverage area (%) quantified by image analysis. Data are presented as mean ± SD from three independent experiments. Compared with the control group, *$p < 0.05$, **$p < 0.01$, ***$p < 0.001$.

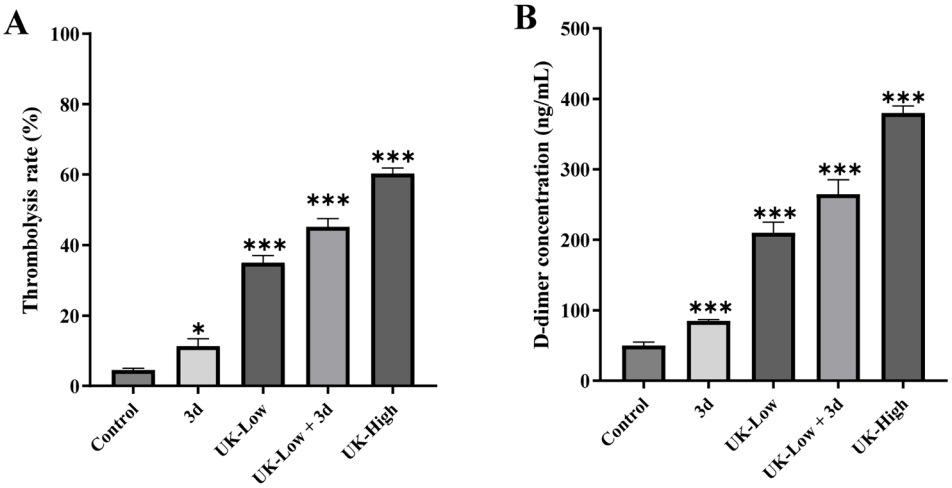

Fig. 7 Synergistic effect of compound **3d** on urokinase thrombolysis. (A) Comparison of thrombolysis rates in different treatment groups; (B) D-dimer levels in the supernatant. Data are presented as mean ± SD from three independent experiments. Compared with the control group, *$p < 0.05$, **$p < 0.01$, ***$p < 0.001$. UK: urokinase.

directed thrombolysis, promising to reduce bleeding risk by decreasing urokinase dosage while accelerating thrombus dissolution and shortening thrombolysis time, providing a new adjunctive therapeutic strategy for the prevention and treatment of in-stent thrombosis.

2.5.6 *In vitro* ADME profiling of compound 3d:plasma protein binding and metabolic stability. The plasma protein binding (PPB) and metabolic stability of compound **3d** were evaluated using equilibrium dialysis and human liver microsome assays, respectively.[48] PPB was determined at three concentrations (1, 5 and 10 μM) and showed concentration-independent binding with a mean value of 89.3%. The metabolic half-life ($t_{1/2}$) in human liver microsomes was 0.754 h, indicating moderate metabolic stability. These data suggest that **3d** possesses acceptable *in vitro* drug-like properties, with approximately 10.7% free fraction and moderate resistance to CYP450-mediated degradation. Detailed results are summarized in Table 3.

Table 3 *In vitro* ADME properties of compound **3d**

Parameter	Value
Plasma protein binding (mean, 1–10 μM)	89.3%
Free fraction	10.7%
Metabolic $t_{1/2}$	0.754 h

2.5.7 Limitations of the *in vitro* approaches. Although compound **3d** showed promising *in vitro* antiplatelet and thrombus-inhibitory activities along with acceptable ADME properties, these findings are strictly limited to *in vitro* systems. The present study did not evaluate *in vivo* antithrombotic efficacy (*e.g.*, in arterial or venous thrombosis models), pharmacokinetics (*e.g.*, bioavailability, plasma clearance), or bleeding risk. Therefore, the *in vivo* translational potential of **3d** remains to be established in appropriate animal models before any clinical application.

2.6 Mechanism of interaction between compound and COX-1

The inhibition rate of compound **3d** against COX-1 was determined at a fixed concentration of 5 μM (approximately 3 times the IC_{50}) in the presence of varying concentrations of arachidonic acid (1, 5, 20 μM). The results showed (Fig. 8A) that as the substrate concentration increased, the inhibition rate decreased in a concentration-dependent manner: when the arachidonic acid concentration was 1 μM, the inhibition rate was 85%; when the concentration increased to 5 μM, the inhibition rate decreased to 60%; when the concentration further increased to 20 μM, the inhibition rate significantly decreased to 35%. This phenomenon is consistent with the typical characteristics of competitive inhibition—the substrate and inhibitor compete for the same active site, and the higher the substrate concentration, the weaker the inhibitor's effect. The inhibition constant (K_i) of compound **3d** against COX-1 was calculated to be 2.8 μM. For comparison, the K_i value of the classic competitive COX-1 inhibitor ibuprofen reported in the literature is 2.5 μM.[49] A smaller K_i value indicates stronger binding affinity of the inhibitor to the enzyme. The K_i value of compound **3d** is slightly higher than that of ibuprofen but still within the range of 1–10 μM, classifying it as a competitive COX-1 inhibitor with moderate affinity (Fig. 8B). This K_i value maintains a good correlation with the COX-1 IC_{50} value and antiplatelet aggregation activity of compound **3d**, indicating that its anti-inflammatory and antithrombotic effects stem from direct inhibition of COX-1.

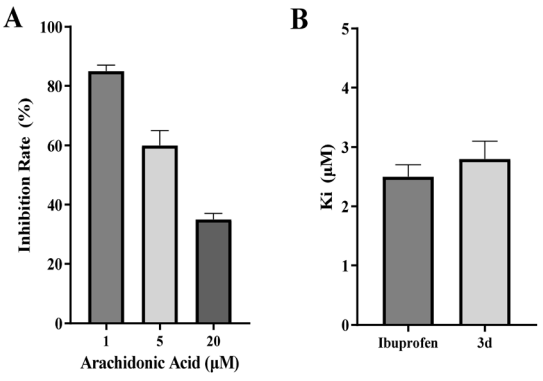

Fig. 8 (A) The inhibition rate of compound **3d** (5 μM) on COX-1 at increasing concentrations of arachidonic acid (1, 5, 20 μM). (B) Comparison of inhibition constants (K_i) of compound **3d** and ibuprofen against COX-1. K_i values were calculated by Dixon plot and nonlinear regression fitting.

2.7 Molecular docking of compound 3d with COX-1

The molecular docking interaction diagram of compound **3d** with COX-1 (PDB ID: 1CQE) (Fig. 9) shows that **3d** binds stably within the arachidonic acid binding pocket.[50] The ligand forms hydrogen bond interactions with the key active-site residue Gln44 and other residues. In addition, the presence of PO-153-related groups around the ligand suggests possible electrostatic complementarity or solvent-mediated indirect interactions. Collectively, these interaction forces anchor **3d** within the substrate channel of COX-1, providing a structural basis for its competitive inhibitory activity.

2.8 Evaluation of antioxidant activity of compound 3d

The antioxidant activity of the target compound **3d** at different concentrations was evaluated using the DPPH radical scavenging assay, and the results are shown in Fig. 10.[51] Compound **3d** scavenged DPPH radicals in a concentration-dependent manner. At concentrations of 25, 50, and 100 μM, the DPPH scavenging rates of **3d** were 15.1%, 27.3%, and 38.0%, respectively. These results indicate that compound **3d** possesses weak direct antioxidant activity, exhibiting only moderate to low free radical scavenging capacity within the concentration range of 25–100 μM. Combined with its strong COX-1 inhibitory activity and antiplatelet aggregation effects, it can be inferred that the anti-inflammatory and antithrombotic effects of **3d** primarily stem from direct inhibition of targets such as COX-1, rather than indirectly through free radical scavenging. This finding is consistent with literature reports: the anti-inflammatory activity of Schiff base compounds is usually directly related to their COX inhibitory capacity, with antioxidant activity not being their primary mechanism of action.

2.9 Structure–activity relationship (SAR) analysis

A qualitative SAR analysis based on the *in vitro* data revealed the following trends: (i) a chloro substituent on the benzohydrazide core (**3a–3f**) generally conferred higher COX-1 inhibitory potency than the methyl analogues (**3g–3l**), suggesting that an electron-withdrawing group enhances binding to COX-1; (ii) among the six aldehyde types, furan- and thiophene-containing

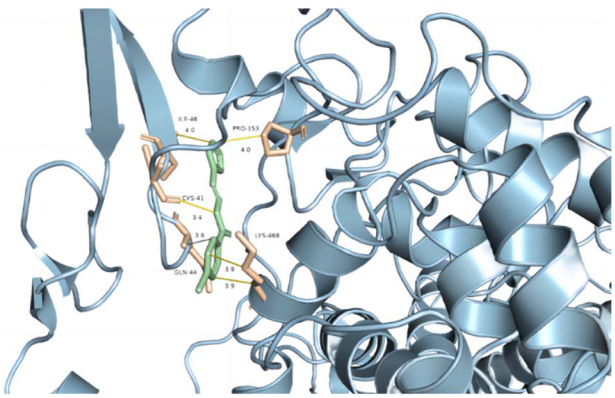

Fig. 9 Molecular docking of **3d** to the putative binding site of the target protein (PDB ID: 1CQE).

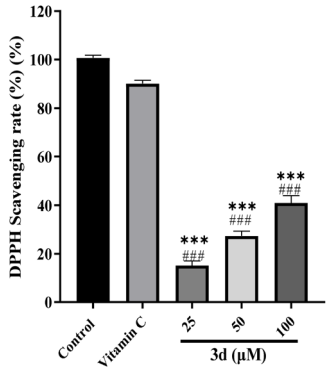

Fig. 10 DPPH radical scavenging activity of compound **3d**. The radical scavenging capacity of compound **3d** at different concentrations was determined using the DPPH assay, with vitamin C (100 μM) as a positive control. Data are presented as mean ± SD from three independent experiments. ***$p < 0.001$ *vs.* vitamin C group.

derivatives (**3d**, **3e**, **3j**, **3k**) exhibited the strongest antiplatelet activity, likely due to heteroatom-mediated interactions within the COX-1 active site; (iii) biphenyl-substituted compounds (**3c**, **3i**) showed good antiplatelet effects but moderate hemolysis, whereas benzoic acid derivatives (**3a**, **3g**) had the lowest antiplatelet activity yet the best hemocompatibility; (iv) pyridine-containing analogues (**3f**, **3l**) displayed moderate activities across all assays. Based on this SAR, compound **3d** (4-chlorobenzohydrazide + furan-2-carbaldehyde) was identified as the lead compound balancing efficacy and safety.

3. Conclusion

In this study, twelve benzohydrazide Schiff base derivatives were synthesized and their *in vitro* anti-inflammatory, antiplatelet, and thrombus-inhibitory activities were systematically evaluated. Among them, compound **3d** was identified as a moderately selective COX-1 inhibitor ($IC_{50} = 1.63$ μM, SI = 8.87) with additional 5-LOX inhibition. It effectively suppressed the release of pro-inflammatory cytokines, inhibited ADP- and collagen-induced platelet aggregation, reduced platelet activation markers, and attenuated thrombus formation under arterial shear. Furthermore, **3d** enhanced the thrombolytic efficacy of low-dose urokinase in a static *in vitro* clot lysis model. A qualitative SAR analysis indicated that the chloro substituent on the benzohydrazide core combined with a furan-containing aldehyde provided an optimal activity-safety profile. These *in vitro* findings suggest that **3d** may hold potential as an adjunctive agent for catheter-directed thrombolysis in in-stent thrombosis. Further *in vivo* evaluation of its antithrombotic efficacy, pharmacokinetics, and bleeding risk is required to establish its translational potential.

4. Experimental section

4.1 Chemical synthesis

4.1.1 Instruments and reagents. All starting materials and reagents were commercially available as analytically pure and were used without further purification. Reaction progress was monitored by thin-layer chromatography (TLC) using silica gel plates and visualized under a UV lamp (254 nm). Melting points of intermediates and target compounds were determined using an X-4 micro melting point apparatus. Proton nuclear magnetic resonance (^{1}H NMR) and carbon-13 nuclear magnetic resonance (^{13}C NMR) spectra were recorded on a Bruker AV-400 NMR spectrometer with tetramethylsilane (TMS) as the internal standard and DMSO-d_6 as the solvent. High-resolution mass spectrometry (HR-MS) was performed using an Agilent 6520 Q-TOF mass spectrometer. Compound purity was analyzed using an Agilent 1260 high-performance liquid chromatography system equipped with a C18 column (4.6 mm × 250 mm, 5 μm).

4.1.2 Synthesis of target compounds 3a–3l. Ethyl *p*-methylbenzoate (10 mmol) and ethyl *p*-chlorobenzoate (10 mmol) were respectively dissolved in anhydrous ethanol (30 mL), and 80% hydrazine hydrate (20 mmol) was added. The mixture was heated under reflux for 6–8 h. After the reaction was complete as monitored by TLC, the mixture was cooled to room temperature, and a white solid precipitated. The solid was collected by suction filtration and recrystallized from ethanol to obtain the intermediates 4-methylbenzohydrazide and 4-chlorobenzohydrazide.

The above intermediates (1 mmol) were dissolved in anhydrous ethanol (15 mL), and equimolar amounts of aromatic aldehydes (4-formylbenzoic acid, 4-hydroxybenzaldehyde, 4-biphenylcarboxaldehyde, furan-2-carbaldehyde, thiophene-2-carbaldehyde, or pyridine-4-carbaldehyde) were added respectively. The mixture was heated under reflux for 4–6 h. After the reaction was complete as monitored by TLC, the mixture was cooled, and a solid precipitated. The solid was collected by suction filtration, washed with ethanol, and dried to obtain the target compounds **3a–3l** in yields ranging from 81% to 93%. All target compounds were characterized by ^{1}H NMR, ^{13}C NMR, and HR-MS to confirm their structures.

4.1.3 4-((2-(4-chlorobenzoyl)hydrazineylidene)methyl)benzoic acid (3a). 258 mg, yield, 83%. White solid powder. M.P. 286 – 289 °C. ^{1}H NMR (400 MHz, DMSO-d6) δ 12.08 (s, 1H), 8.52 (s, 1H), 8.01 (m, 4H), 7.87 (d, $J = 7.8$ Hz, 2H), 7.63 (d, $J = 8.1$ Hz, 2H). ^{13}C NMR (101 MHz, DMSO-d_6) δ 166.68, 162.02, 146.71, 138.05, 136.54, 129.58, 129.41, 128.40, 126.93, 39.52. TOF-MS, *m*/*z*: $[M + H]^+$, calcd. for $C_{15}H_{12}ClN_2O_3^+$, 303.0536, found: 303.0541.

4.1.3.1 4-Chloro-N′-(4-hydroxybenzylidene)benzohydrazide (3b). 227 mg, yield, 83%. White solid powder. M.P. 204 – 206 °C. ^{1}H NMR (400 MHz, DMSO-d_6) δ 11.74 (s, 1H), 9.97 (s, 1H), 8.37 (s, 1H), 7.95 (d, $J = 8.4$ Hz, 2H), 7.60 (*t*, $J = 8.0$ Hz, 4*H*), 6.87 (d, $J = 8.4$ Hz, 2H).^{13}C NMR (101 MHz, DMSO-d_6) δ 161.83, 159.53, 148.51, 136.41, 132.36, 129.48, 128.94, 128.53, 125.22, 115.75. TOF-MS, *m*/*z*: [M + H]+, calcd. for $C_{14}H_{12}ClN_2O_2^+$, 275.0587, found: 275.0592.

4.1.4 *N′*-([1,1′-biphenyl]-4-ylmethylene)-4-chlorobenzohydrazide (3c). 294 mg, yield, 88%. M.P. 187 – 189 °C. ^{1}H NMR (400 MHz, DMSO-d_6) δ 11.98 (s, 1H), 8.53 (s, 1H), 7.99 (d, $J = 8.1$ Hz, 2H), 7.90–7.71 (m, 5*H*), 7.64 (d, $J = 8.2$ Hz, 2H), 7.50 (d, $J = 7.5$ Hz, 2H), 7.42 (s, 1H). ^{13}C NMR (101 MHz, DMSO-d_6) δ 162.05, 147.68, 141.64, 139.30, 136.59, 133.33, 132.12, 129.55, 129.01, 128.57, 127.05, 126.66, 39.52. TOF-MS,

m/z: $[M + H]^+$, calcd. for $C_{20}H_{16}ClN_2O^+$, 335.0943, found: 335.0948.

4.1.5 4-Chloro-*N*′-(furan-2-ylmethylene)benzohydrazide (3d). 211 mg, yield, 85%. White solid powder. M.P. 239 – 241 °C. ^{1}H NMR (400 MHz, DMSO-d_6) δ 11.88 (s, 1H), 8.36 (s, 1H), 7.95 (d, J = 8.3 Hz, 2H), 7.86 (s, 1H), 7.61 (d, J = 8.3 Hz, 2H), 6.95 (s, 1H), 6.65 (s, 1H). ^{13}C NMR (101 MHz, DMSO-d_6) δ 162.23, 149.58, 145.47, 138.09, 136.82, 132.25, 129.71, 128.78, 113.91, 112.42, 39.52. TOF-MS, *m/z*: $[M + H]^+$, calcd. for $C_{12}H_{10}ClN_2O_2^+$, 249.0431, found: 249.0434.

4.1.6 4-Chloro-*N*′-(thiophen-2-ylmethylene) benzohydrazide (3e). 230 mg, yield, 87%. White solid powder. M.P. 197 – 199 °C. ^{1}H NMR (400 MHz, DMSO-d_6) δ 11.86 (s, 1H), 8.65 (s, 1H), 7.91 (d, J = 8.3 Hz, 2H), 7.65 (s, 1H), 7.57 (d, J = 8.3 Hz, 2H), 7.45 (s, 1H), 7.12 (s, 1H). ^{13}C NMR (101 MHz, DMSO-d_6) δ 162.16, 143.47, 139.22, 136.80, 132.29, 131.28, 129.70, 129.27, 128.77, 128.06, 39.52. TOF-MS, *m/z*: $[M + H]^+$, calcd. for $C_{12}H_{10}ClN_2OS^+$, 265.0202, found: 265.0204.

4.1.7 4- chloro-*N*′-(pyridin-4-ylmethylene)benzohydrazide (3f). 231 mg, yield, 89%. White solid powder. M.P. 201 – 203 °C. ^{1}H NMR (400 MHz, DMSO-d_6) δ 12.16 (s, 1H), 8.62 (s, 2H), 8.41 (s, 1H), 7.93 (d, J = 7.9 Hz, 2H), 7.73–7.44 (m, 4H). ^{13}C NMR (101 MHz, DMSO-d_6) δ 162.67, 151.31, 150.49, 145.94, 141.64, 137.18, 129.91, 128.88, 121.28. TOF-MS, *m/z*: $[M + H]^+$, calcd. for $C_{13}H_{11}ClN_3O^+$, 260.0590, found: 260.0594.

4.1.8 4-((2-(4-methylbenzoyl)hydrazineylidene)methyl)benzoic acid (3g). 254 mg, yield, 90%. White solid powder. M.P. 260 – 262 °C. ^{1}H NMR (400 MHz, DMSO-d_6) δ 11.91 (s, 1H), 8.49 (s, 1H), 7.99 (d, J = 7.9 Hz, 2H), 7.81 (s, 3H), 7.31 (d, J = 7.9 Hz, 2H), 2.35 (s, 3H). ^{13}C NMR (101 MHz, DMSO-d_6) δ 167.10, 163.32, 146.70, 142.16, 138.65, 131.87, 129.98, 129.21, 127.90, 127.23, 39.52, 21.23. TOF-MS, *m/z*: $[M + H]^+$, calcd. for $C_{16}H_{15}N_2O_3^+$, 283.1082, found: 283.1084.

4.1.9 *N*′-(4-hydroxybenzylidene)-4-methylbenzohydrazide (3h). 224 mg, yield, 88%. White solid powder. M.P. 197 – 199 °C. ^{1}H NMR (400 MHz, DMSO-d_6) δ 11.56 (s, 1H), 9.89 (s, 1H), 8.34 (s, 1H), 7.80 (d, J = 7.8 Hz, 2H), 7.54 (d, J = 8.3 Hz, 2H), 7.28 (s, 2H), 6.82 (d, J = 8.3 Hz, 2H), 2.34 (s, 3H). ^{13}C NMR (101 MHz, DMSO-d_6) δ 159.57, 148.10, 141.73, 130.97, 129.12, 127.73, 115.90, 39.52, 21.19. TOF-MS, *m/z*: $[M + H]^+$, calcd. for $C_{15}H_{15}N_2O_2^+$, 255.1133, found: 255.1136.

4.1.10 *N*′-([1,1′-biphenyl]-4-ylmethylene)-4-methylbenzohydrazide (3i). 292 mg, yield, 93%. White solid powder. M.P. 186 – 189 °C. ^{1}H NMR (400 MHz, DMSO-d_6) δ 11.83 (s, 1H), 8.43 (s, 1H), 7.90–7.65 (m, 4H), 7.48 (d, J = 8.1 Hz, 2H), 7.30 (d, J = 7.8 Hz, 2H), 2.35 (s, 3H). ^{13}C NMR (101 MHz, DMSO-d_6) δ 163.22, 146.37, 142.05, 134.62, 133.55, 130.64, 129.17, 128.83, 127.84, 39.52, 21.20. TOF-MS, *m/z*: $[M + H]^+$, calcd. for $C_{21}H_{19}N_2O^+$, 315.1497, found: 315.1501.

4.1.11 *N*′-(furan-2-ylmethylene)-4-methylbenzohydrazide (3j). 196 mg, yield, 86%. White solid powder. M.P. 210 – 212 °C. ^{1}H NMR (400 MHz, DMSO-d_6) δ 11.71 (s, 1H), 8.33 (s, 1H), 7.92–7.71 (m, 3H), 7.30 (d, J = 7.8 Hz, 2H), 6.90 (s, 1H), 6.61 (s, 1H), 2.34 (s, 3H). ^{13}C NMR (101 MHz, DMSO-d_6) δ 163.11, 149.73, 145.27, 142.00, 137.54, 130.67, 129.18, 127.78, 113.45, 112.36, 21.20. TOF-MS, *m/z*: $[M + H]^+$, calcd. for $C_{13}H_{13}N_2O_2^+$, 229.0977, found: 229.0980.

4.1.12 4-Methyl-*N*′-(thiophen-2-ylmethylene) benzohydrazide (3k). 212 mg, yield, 87%. White solid powder. M.P. 185 – 188 °C. ^{1}H NMR (400 MHz, DMSO-d_6) δ 11.74 (s, 1H), 8.67 (s, 1H), 7.80 (d, J = 7.8 Hz, 2H), 7.64 (s, 1H), 7.43 (s, 1H), 7.29 (d, J = 7.8 Hz, 2H), 7.12 (s, 1H), 2.34 (s, 3H). ^{13}C NMR (101 MHz, DMSO-d_6) δ 162.89, 142.71, 139.22, 130.74, 128.98, 127.82, 127.58, 21.01. TOF-MS, *m/z*: $[M + H]^+$, calcd. for $C_{13}H_{13}N_2OS^+$, 245.0748, found: 245.0752.

4.1.13 4-Methyl-*N*′-(pyridin-4-ylmethylene)benzohydrazide (3l). 215 mg, yield, 90%. White solid powder. M.P. 193 – 196 °C. ^{1}H NMR (400 MHz, DMSO-d_6) δ 12.03 (s, 1H), 8.62 (s, 2H), 8.43 (s, 1H), 7.83 (d, J = 7.2 Hz, 2H), 7.63 (s, 2H), 7.31 (d, J = 7.9 Hz, 2H), 2.35 (s, 3H). ^{13}C NMR (101 MHz, DMSO-d_6) δ 150.45, 145.26, 129.25, 127.98, 121.16, 21.18. TOF-MS, *m/z*: $[M + H]^+$, calcd. for $C_{14}H_{14}N_3O^+$, 240.1137, found: 240.1140.

4.2 Cellular safety evaluation

4.2.1 Cytotoxicity detection by MTT assay. Mouse macrophage RAW264.7 cells were purchased from the Cell Bank of the Chinese Academy of Sciences and cultured in DMEM high-glucose medium containing 10% fetal bovine serum (FBS), 100 U per mL penicillin, and 100 μg mL^{-1} streptomycin in a 37 °C incubator with 5% CO_2.[37] RAW264.7 cells in logarithmic growth phase were seeded into 96-well plates at a density of 1 × 10^4 cells per well. After 24 h of culture, different concentrations (5, 25, 50, 100, 200 μM) of the test compounds (**3a–3l**) were added, with three replicate wells set for each concentration. A solvent control group (0.1% DMSO) and a blank control group were also established. After continued incubation for 24 h, 20 μL of MTT solution (5 mg mL^{-1}) was added to each well and incubated for 4 h. The supernatant was discarded, and 150 μL of DMSO was added to dissolve the formazan crystals. The absorbance (OD value) was measured at 490 nm using a microplate reader. Cell viability (%) = ($OD_{experimental\ group}$ − $OD_{blank\ group}$)/($OD_{control\ group}$ − $OD_{blank\ group}$) × 100%.

4.2.2 Erythrocyte hemolysis assay. Fresh human anticoagulated blood (Merck) was obtained commercially, and erythrocytes were isolated by centrifugation, washed three times with physiological saline, and prepared as a 2% erythrocyte suspension.[38] Different concentrations (25, 50, 100 μM) of the test compounds were mixed with an equal volume of erythrocyte suspension and incubated at 37 °C for 1 h. After centrifugation, the supernatant was collected, and the absorbance was measured at 540 nm. A 0.1% DMSO solution was used as the negative control, and 1% Triton X-100 was used as the positive control. Hemolysis rate (%) = (OD_{sample} − $OD_{negative\ control}$)/($OD_{positive\ control}$ − $OD_{negative\ control}$) × 100%.

4.3 Determination of COX-1/COX-2/5-LOX inhibitory activity

The inhibitory activities of the compounds against COX-1, COX-2, and 5-LOX were determined using corresponding enzyme activity assay kits (purchased from Beyotime Biotechnology Co., Ltd.).[39] Experiments were performed according to the kit instructions. Blank control, positive control (celecoxib for COX-2, zileuton for 5-LOX), and test compound groups at different concentrations were set up respectively. The half-maximal

inhibitory concentrations (IC_{50}) of each compound against the three enzymes were calculated, and the COX-1 selectivity index (SI = COX-2 IC_{50}/COX-1 IC_{50}) was determined.

4.4 Evaluation of anti-inflammatory activity

RAW264.7 cells in logarithmic growth phase were seeded into 24-well plates at a density of 2×10^5 cells per well. After 24 h of culture, different concentrations (25, 50, 100 μM) of compound **3d** or **3e** were added for pretreatment for 1 h, followed by stimulation with LPS (final concentration 1 μg mL^{-1}) for 24 h.[40] A blank control group (without LPS stimulation) and a model control group (LPS stimulation only) were established. Three replicate wells were set for each group. Cell culture supernatants were collected, and the levels of TNF-α, IL-6, IL-1β, and PGE_2 in the supernatants were determined using ELISA kits (purchased from R&D Systems Biotechnology Co., Ltd) according to the manufacturer's instructions.

4.5 Evaluation of platelet function

4.5.1 Platelet aggregation assay. Fresh human whole blood was obtained commercially (Keyuan Xin Biotechnology Co., Ltd). Platelet-rich plasma (PRP) was prepared by centrifugation at 200 × *g* for 10 min, and platelet-poor plasma (PPP) was prepared by centrifuging the remaining blood at 2000 × *g* for 10 min. Platelet aggregation rates were measured using the turbidimetric method on a platelet aggregometer.[41] PRP was pre-incubated with different concentrations of compound **3d** or **3e** for 15 min, then ADP (final concentration 10 μM) or collagen (final concentration 2 μg mL^{-1}) was added to induce platelet aggregation. Aggregation was continuously recorded for 5 min, with PPP used as a blank. Inhibition rates were calculated, and IC_{50} values were determined. For arachidonic acid (AA)-induced aggregation, AA (final concentration 1 mM, Sigma-Aldrich) was added to PRP after pre-incubation with compound **3d**, **3e** or aspirin for 15 min at 37 °C. Aggregation was recorded for 5 min, and IC_{50} values were calculated as described above.

4.5.2 Detection of platelet activation markers. PRP was pre-incubated with different concentrations of compound **3d** (12.5, 25, 50 μM) for 15 min, followed by activation with ADP (10 μM) for 10 min.[43] FITC-labeled anti-human CD62P antibody and PAC-1 antibody were added respectively and incubated in the dark for 20 min. After dilution with PBS, samples were immediately analyzed using a flow cytometer. A total of 10 000 platelets were collected for each sample, and the CD62P positivity rate and PAC-1 binding rate were calculated.

4.6 Whole blood thrombus formation assay

Fresh human whole blood was obtained commercially (Keyuan Xin Biotechnology Co., Ltd). Compound **3d** at different concentrations (25, 50, 100 μM) was added to 1 mL aliquots of whole blood and mixed thoroughly. Subsequently, 340 μL of the mixture was transferred to the test cup of a thromboelastography analyzer, and the reaction time (*R* time), clotting time (*K* time), α angle, and maximum amplitude (MA value) were measured according to the instrument operating procedures. An equal volume of physiological saline was added to the control group.[44]

4.7 *In vitro* thrombolytic synergy experiment

PRP was mixed with thrombin (final concentration 10 U per mL) and $CaCl_2$ (final concentration 20 mM), immediately mixed thoroughly, and added to 96-well plates at 100 μL per well. The plates were incubated at 37 °C for 2 h to form stable platelet-rich thrombi. The initial weight of the thrombi in each well was recorded. The thrombi were randomly divided into 6 groups: control group (saline), low-dose urokinase group (100 IU per mL), high-dose urokinase group (500 IU per mL), **3d** monotherapy group (50 μM), low-dose combination group (100 IU per mL urokinase + 50 μM **3d**), and high–dose combination group (500 IU per mL urokinase + 50 μM **3d**). Corresponding reagents (100 μL) were added to each well and incubated at 37 °C for 2 h.

After incubation, the supernatant was discarded, and the remaining thrombus weight was measured. The thrombolysis rate was calculated as follows: thrombolysis rate (%) = (initial weight – remaining weight)/initial weight × 100%. The supernatant was collected, and D-dimer levels were detected using an ELISA kit according to the manufacturer's instructions.[46,47]

4.8 Study on COX-1 inhibition mechanism

With a fixed concentration of compound **3d** at 5 μM, enzyme activity was measured using the COX-1 activity assay kit in the presence of different concentrations of arachidonic acid (1, 5, 20 μM), and the inhibition rates were calculated.[49] A series of different concentrations of arachidonic acid (1, 2, 5, 10, 20 μM) and different concentrations of compound **3d** (0, 0.5, 1, 2, 4 μM) were set up to determine COX-1 enzyme activity. The K_i value was calculated using Dixon plot analysis and nonlinear regression fitting.

4.9 Evaluation of antioxidant activity (DPPH scavenging assay)

Compound **3d** was dissolved in anhydrous ethanol to prepare different concentrations (25, 50, 100 μM). An aliquot of 100 μL of the sample solution was mixed with 100 μL of DPPH ethanol solution (0.1 mM) and incubated at room temperature in the dark for 30 min. The absorbance was measured at 517 nm. Vitamin C (100 μM) was used as a positive control.[50] DPPH scavenging rate (%) = (A_blank – A_sample)/A_blank × 100%.

4.10 Parallel-plate flow chamber assay

Glass coverslips were coated with 200 μg mL^{-1} type I collagen overnight at 4 °C, then blocked with 1% BSA for 1 h. The coverslip was assembled into a parallel-plate flow chamber. Human whole blood (citrated) was recalcified with 10 mM $CaCl_2$, pre-incubated with compound **3d** (25–100 μM) or 0.1% DMSO for 5 min at 37 °C, and perfused through the chamber at a shear rate of 1000 s^{-1} for 5 min. After flushing with PBS, thrombus formation was quantified by measuring protein content (BCA assay) and platelet coverage area (bright-field

microscopy with ImageJ). Experiments were performed in triplicate using blood from three independent donors.[45]

4.11 Plasma protein binding assay

Compound **3d** was spiked into human plasma at 1, 5 and 10 μM (0.1% DMSO). Aliquots (200 μL) were dialyzed against PBS (pH 7.4) using a 96-well RED device at 37 °C for 6 h with shaking. After dialysis, samples from both chambers were mixed with acetonitrile containing internal standard, centrifuged, and analyzed by LC-MS/MS. PPB (%) was calculated as $(C_{plasma} - C_{buffer})/C_{plasma} \times 100\%$. Each concentration was tested in triplicate.[48]

4.12 Metabolic stability assay

Compound **3d** (1 μM) was incubated with pooled human liver microsomes (0.5 mg mL^{-1}) and 1 mM NADPH at 37 °C (BIOSCIENCE). At 0, 5, 15, 30, 45 and 60 min, aliquots were withdrawn and terminated with ice-cold acetonitrile containing internal standard. After centrifugation, supernatants were analyzed by LC-MS/MS. The half-life ($t_{1/2}$) was calculated from the ln(remaining fraction) *vs.* time plot.[48]

4.13 Molecular docking analysis

The three-dimensional structure of COX-1 was retrieved from the RCSB Protein Data Bank (PDB ID: 1CQE). Protein preparation was carried out using molecular docking software, including removal of water molecules and the original ligand, addition of polar hydrogens, and assignment of partial charges. The three-dimensional structure of compound **3d** was built with molecular modeling tools and energy-minimized. Docking was performed using a semi-flexible docking method, with a grid box defined to cover the arachidonic acid binding pocket. The conformation with the lowest binding energy was selected for interaction analysis. The docking protocol was validated by re-docking the co-crystallized ligand into the binding site.[50]

4.14 Statistical analysis

All experimental data were expressed as mean ± SD or mean ± SEM. Statistical analysis was performed using GraphPad Prism 8.0 software. Comparisons among multiple groups were conducted using one-way analysis of variance (ANOVA) followed by Dunnett's test, and comparisons between two groups were performed using Student's *t*-test. A value of $p < 0.05$ was considered statistically significant.

Conflicts of interest

The authors declare that the research was conducted in the absence of any commercial or financial relationships that could be construed as a potential conflict of interest.

Data availability

Data will be made available on request.

Supplementary information (SI) is available. See DOI: https://doi.org/10.1039/d6ra01870j.

Acknowledgements

Cangzhou's Self-funded Projects under the Science and Technology Program (Project No. 23244102019) — Application value of balloon pre-dilation combined with catheter-directed thrombolysis in lower extremity arterial in-stent thrombosis.

References

1 J. P. Salazar Adum, I. Golemi, L. H. Paz, L. Diaz Quintero, A. J. Tafur and J. A. Caprini, Venous thromboembolism controversies, *Disease-a-Month*, 2018, **64**, 408–444, DOI: 10.1016/j.disamonth.2018.03.003.

2 M. P. Winter, G. H. Schernthaner and I. M. Lang, Chronic complications of venous thromboembolism, *J. Thromb. Haemost.*, 2017, **15**, 1531–1540, DOI: 10.1111/jth.13741.

3 F. Khan, T. Tritschler, S. R. Kahn and M. A. Rodger, Venous thromboembolism, *Lancet*, 2021, **398**, 64–77, DOI: 10.1016/S0140-6736(20)32658-1.

4 Z. Zhang, L. Tang and Y. Hu, Progress in the research on venous thromboembolism, *J. Huazhong Univ. Sci. Technol. - Med. Sci.*, 2017, **37**, 811–815, DOI: 10.1007/s11596-017-1811-z.

5 P. Prandoni, The Treatment of Venous Thromboembolism in Patients with Cancer, *Adv. Exp. Med. Biol.*, 2017, **906**, 123–135, DOI: 10.1007/5584_2016_111.

6 J. B. Wetmore, C. A. Herzog, H. Yan, J. L. Reyes, E. D. Weinhandl and N. S. Roetker, Apixaban versus Warfarin for Treatment of Venous Thromboembolism in Patients Receiving Long-Term Dialysis, *Clin. J. Am. Soc. Nephrol.*, 2022, **17**, 693–702, DOI: 10.2215/CJN.14021021.

7 K. Stark and S. Massberg, Interplay between inflammation and thrombosis in cardiovascular pathology, *Nat. Rev. Cardiol.*, 2021, **18**, 666–682, DOI: 10.1038/s41569-021-00552-1.

8 S. P. McAdoo and N. Dhaun, Resolving thromboinflammation, *Blood*, 2021, **137**, 1444–1446, DOI: 10.1182/blood.2020010627.

9 K. N. Ekdahl, S. Huang, B. Nilsson and Y. Teramura, Complement inhibition in biomaterial- and biosurface-induced thromboinflammation, *Semin. Immunol.*, 2016, **28**, 268–277, DOI: 10.1016/j.smim.2016.04.006.

10 J. Li and J. Cho, Ser/Thr protein kinase Bβ-NADPH oxidase 2 signaling in thromboinflammation, *Curr. Opin. Hematol.*, 2017, **24**, 460–466, DOI: 10.1097/MOH.0000000000000365.

11 A. Dupuy, L. Hagimola, N. S. A. Mgaieth, C. B. Houlahan, R. E. Preketes-Tardiani, P. R. Coleman and F. H. Passam, Thromboinflammation Model-on-A-Chip by Whole Blood Microfluidics on Fixed Human Endothelium, *Diagnostics*, 2021, **11**, 203, DOI: 10.3390/diagnostics11020203.

12 H. Zhang, L. Wang, Y. Yang, C. Cai, X. Wang, L. Deng, B. He, W. Zhou and Y. Cui, DL-3-n-butylphthalide (NBP) alleviates poststroke cognitive impairment (PSCI) by suppressing neuroinflammation and oxidative stress, *Front. Pharmacol*, 2023, **13**, 987293, DOI: 10.3389/fphar.2022.987293.

13 W. Fang, W. Sun, W. Fang, S. Zhao and C. Wang, Clinical features, treatment, and outcomes of patients with

carfilzomib induced thrombotic microangiopathy, *Int. Immunopharmacol.*, 2024, **134**, 112178, DOI: 10.1016/j.intimp.2024.112178.

14 R. Dinc, A review of the current state in neointimal hyperplasia development following endovascular intervention and minor emphasis on new horizons in immunotherapy, *Transl. Clin. Pharmacol.*, 2023, **31**, 191–201, DOI: 10.12793/tcp.2023.31.e18.

15 S. Xu, J. Xing, L. Zheng, H. Su, Y. Zou, Y. Niu and H. Di, Azithromycin regulates Mettl3-mediated NF-κB pathway to enhance M2 polarization of RAW264.7 macrophages and attenuate LPS-triggered cytotoxicity of MLE-12 alveolar cells, *Int. Immunopharmacol.*, 2024, **137**, 112426, DOI: 10.1016/j.intimp.2024.112426.

16 M. Crescente, L. Menke, M. V. Chan, P. C. Armstrong and T. D. Warner, Eicosanoids in platelets and the effect of their modulation by aspirin in the cardiovascular system (and beyond), *Br. J. Pharmacol.*, 2019, **176**, 988–999, DOI: 10.1111/bph.14196.

17 J. A. Mitchell, N. S. Kirkby, B. Ahmetaj-Shala, P. C. Armstrong, M. Crescente, P. Ferreira, M. E. Lopes Pires, R. Vaja and T. D. Warner, Cyclooxygenases and the cardiovascular system, *Pharmacol. Ther.*, 2021, **217**, 107624, DOI: 10.1016/j.pharmthera.2020.107624.

18 R. B. Raffa, J. A. Gudin, S. Nalamachu and J. V. Pergolizzi Jr., Selective' COX-1 or COX-2 NSAIDs: time to change a misleading measure, *Int. J. Clin. Pharm. Ther.*, 2014, **39**, 455–456, DOI: 10.1111/jcpt.12192.

19 Z. Suo, Y. Liu, Y. Li, C. Xu, Y. Liu, M. Gao and J. Dong, Calcitriol inhibits COX-1 and COX-2 expressions of renal vasculature in hypertension: Reactive oxygen species involved?, *Clin. Exp. Hypertens.*, 2021, **43**, 91–100, DOI: 10.1080/10641963.2020.1817473.

20 X. Sun and Q. Li, Prostaglandin EP2 receptor: Novel therapeutic target for human cancers, *Int. J. Mol. Med.*, 2018, **42**, 1203–1214, DOI: 10.3892/ijmm.2018.3744.

21 T. Gremmel, A. L. Frelinger 3rd and A. D. Michelson, Platelet Physiology, *Semin. Thromb. Hemost.*, 2016, **42**, 191–204, DOI: 10.1055/s-0035-1564835.

22 M. K. Nayak, M. Ghatge, G. D. Flora, N. Dhanesha, M. Jain, K. R. Markan, M. J. Potthoff, S. R. Lentz and A. K. Chauhan, The metabolic enzyme pyruvate kinase M2 regulates platelet function and arterial thrombosis, *Blood*, 2021, **137**, 1658–1668, DOI: 10.1182/blood.2020007140.

23 L. Chen, Z. Jiang, L. Yang, Y. Fang, S. Lu, O. U. Akakuru, S. Huang, J. Li, S. Ma and A. Wu, HPDA/Zn as a CREB Inhibitor for Ultrasound Imaging and Stabilization of Atherosclerosis Plaque, *Chin. J. Chem.*, 2023, **41**, 199–206, DOI: 10.1002/cjoc.202200406.

24 W. Liu, G. Li, J. Shi, Y. Gao, P. Fang, Y. Zhao, F. Zhong, X. Guo, Y. Lyu, X. Da, Z. Li, J. Fa, L. Hu, A. Yuan, L. Chen, J. Liu, A. F. Chen, B. Sheng, Y. Ji, X. Lu and J. Pu, NR4A1 Acts as a Novel Regulator of Platelet Activation and Thrombus Formation, *Circ. Res.*, 2025, **136**, 809–826, DOI: 10.1161/CIRCRESAHA.124.325645.

25 P. M. Ridker, B. M. Everett, T. Thuren, J. G. MacFadyen, W. H. Chang, C. Ballantyne, F. Fonseca, J. Nicolau, W. Koenig, S. D. Anker, J. J. P. Kastelein, J. H. Cornel, P. Pais, D. Pella, J. Genest, R. Cifkova, A. Lorenzatti, T. Forster, Z. Kobalava, L. Vida-Simiti, M. Flather, H. Shimokawa, H. Ogawa, M. Dellborg, P. R. F. Rossi, R. P. T. Troquay, P. Libby and R. J. Glynn, the CANTOS Trial Group, Antiinflammatory Therapy with Canakinumab for Atherosclerotic Disease, *N. Engl. J. Med.*, 2017, **377**, 1119–1131, DOI: 10.1056/NEJMoa1707914.

26 H. Wang, C. Tang, Y. Xiang, C. Zou, J. Hu, G. Yang and W. Zhou, Tea polyphenol-derived nanomedicine for targeted photothermal thrombolysis and inflammation suppression, *J. Nanobiotechnol.*, 2024, **22**, 146, DOI: 10.1186/s12951-024-02446-z.

27 Y. Feng, B. Wang, N. Zhao, G. Zhang, B. Lu and S. Li, Multimodal computed tomography-guided mechanical thrombectomy for large vessel occlusion stroke after cardiac surgery, *Brain Heart*, 2025, **3**, 4141, DOI: 10.36922/bh.4141.

28 Y. Khan, H. Sarfraz, W. Rehman, M. Khan, L. Rasheed and K. U. Rahman, Innovative Horizons in Drug Design: Exploring the Synthesis and Medicinal Properties of Heterocyclic Schiff Bases. A Review, *Mini Rev. Med. Chem.*, 2025, **25**, 727–744, DOI: 10.2174/0113895575320413250126041041.

29 Y. Sun, Y. Lu, M. Bian, Z. Yang, X. Ma and W. Liu, Pt(II) and Au(III) complexes containing Schiff-base ligands: A promising source for antitumor treatment, *Eur. J. Med. Chem.*, 2021, **211**, 113098, DOI: 10.1016/j.ejmech.2020.113098.

30 V. R. Mishra, C. W. Ghanavatkar, S. N. Mali, H. K. Chaudhari and N. Sekar, Schiff base clubbed benzothiazole: synthesis, potent antimicrobial and MCF-7 anticancer activity, DNA cleavage and computational study, *J. Biomol. Struct. Dyn.*, 2020, **38**, 1772–1785, DOI: 10.1080/07391102.2019.1621213.

31 P. F. Lamie, W. A. M. Ali, V. Bazgier and L. Rárová, Novel N-substituted indole Schiff bases as dual inhibitors of cyclooxygenase-2 and 5-lipoxygenase enzymes: Synthesis, biological activities *in vitro* and docking study, *Eur. J. Med. Chem.*, 2016, **123**, 803–813, DOI: 10.1016/j.ejmech.2016.08.013.

32 N. Kalhor, M. Mardani, S. Abdollahzadeh, M. Vakof, M. Esfahani Zadeh, K. H. M. E. Tehrani, F. Kobarfard and S. Mohebbi, Novel N-Substituted ((1H-indol-3-yl)methylene) benzohydrazides and ((1H-indol-3-yl)methylene)-2-phenylhydrazines: Synthesis and Antiplatelet Aggregation Activity, *Bull. Korean Chem. Soc.*, 2015, **36**, 2632–2639, DOI: 10.1002/bkcs.10531.

33 M. Yu, C. Dai, J. Shi and J. Fu, Immune modulation strategies to reduce in-stent restenosis, *Biomater. Sci.*, 2025, **13**, 4898–4915, DOI: 10.1039/D5BM00687B.

34 P. F. Lamie, W. A. M. Ali, V. Bazgier and L. Rárová, Novel N-substituted indole Schiff bases as dual inhibitors of cyclooxygenase-2 and 5-lipoxygenase enzymes: Synthesis, biological activities *in vitro* and docking study, *Eur. J. Med. Chem.*, 2016, **123**, 803–813, DOI: 10.1016/j.ejmech.2016.08.013.

35 P. R. Khan, M. Durgaprasad, S. G. Reddy, *et al.*, IBX/KI Promoted Synthesis of 2,5-Disubstituted 1,3,4-Oxadiazoles, *Lett. Org. Chem.*, 2017, 15, DOI: 10.2174/1570178614666170811150216.

36 S. S. Clinton, R. Ramesh and J. G. Maecki, Concise access to perimidines by palladium (II) complexes via acceptorless dehydrogenative coupling of alcohols, *Appl. Organomet. Chem.*, 2022, **36**, e6708, DOI: 10.1002/aoc.6708.

37 L. H. Al-Wahaibi, H. A. Abou-Zied, M. A. Mahmoud, B. G. M. Youssif, S. Bräse and S. M. Rabea, Design, synthesis, and antiproliferative activity of new 5-ethylsulfonyl-indazole-3-carbohydrazides as dual EGFR/VEGFR-2 kinases inhibitors, *J. Enzyme Inhib. Med. Chem.*, 2025, **40**, 2516075, DOI: 10.1080/14756366.2025.2516075.

38 W. Sun, J. Li, J. Zhong, J. Feng, Z. Ye, Y. Lin, W. Su, S. Zhu, Y. Li and W. Jia, Exploring the effect of hydroxyapatite nanoparticle shape on red blood cells and blood coagulation, *Nanomedicine*, 2024, **19**, 2301–2314, DOI: 10.1080/17435889.2024.2396152.

39 L. Kan, E. Capuano, V. Fogliano, R. Verkerk, J. J. Mes, M. M. M. Tomassen and T. Oliviero, Inhibition of α-glucosidases by tea polyphenols in rat intestinal extract and Caco-2 cells grown on Transwell, *Food Chem.*, 2021, **361**, 130047, DOI: 10.1016/j.foodchem.2021.130047.

40 Y. Ma, Y. Ren, Z. J. Dai, C. J. Wu, Y. H. Ji and J. Xu, IL-6, IL-8 and TNF-α levels correlate with disease stage in breast cancer patients, *Adv. Clin. Exp. Med.*, 2017, **26**, 421–426, DOI: 10.17219/acem/62120.

41 L. Zhao, D. Liu, B. Liu, H. Hu and W. Cui, Effects of atorvastatin on ADP-, arachidonic acid-, collagen-, and epinephrine-induced platelet aggregation, *J. Int. Med. Res.*, 2017, **45**, 82–88, DOI: 10.1177/0300060516675681.

42 J. Lei, Y. Zhou, D. Xie and Y. Zhang, Mechanistic insights into a classic wonder drug—aspirin, *J. Am. Chem. Soc.*, 2015, **137**, 70–73, DOI: 10.1021/jacs.5b00479.

43 S. Tsimikas, A. Kille, K. Kaier, T. Nührenberg, K. Franke, C. M. Valina, X. Yang, G. Leibundgut, F. J. Neumann, D. Westermann and W. Hochholzer, Oxidized Phospholipids on ApoB-100, Platelet Activation and Reactivity, and Long-Term Cardiovascular Outcomes, *Arterioscler. Thromb. Vasc. Biol.*, 2025, **45**, 1935–1944, DOI: 10.1161/ATVBAHA.125.322347.

44 N. J. Vollmer, N. A. Leshko, C. S. Wilson and B. W. Gilbert, A Review of Thromboelastography for Nurses, *Crit. Care Nurse*, 2023, **43**, 29–37, DOI: 10.4037/ccn2023371.

45 R. Van Kruchten, J. M. E. M. Cosemans and J. W. M. Heemskerk, Measurement of whole blood thrombus formation using parallel-plate flow chambers – a practical guide, *Platelets*, 2012, **23**, 229–242, DOI: 10.3109/09537104.2011.630848.

46 H. Ullrich, T. Münzel and T. Gori, Coronary Stent Thrombosis- Predictors and Prevention, *Dtsch. Ärztebl. Int.*, 2020, **117**, 320–326, DOI: 10.3238/arztebl.2020.0320.

47 S. Kuramitsu, S. Sonoda, K. Ando, H. Otake, M. Natsuaki, R. Anai, Y. Honda, K. Kadota, Y. Kobayashi and T. Kimura, Drug-eluting stent thrombosis: current and future perspectives, *Cardiovasc. Interv. Ther.*, 2021, **36**, 158–168, DOI: 10.1007/s12928-021-00754-x.

48 D. Gogola, S. Novak Ratajczak, E. Gabor-Worwa, M. Puzio, M. Bochenek, B. Kusznierewicz and J. Wietrzyk, Implementation of a novel method for the determination of plasma protein binding of highly bound compounds using the equilibrium dialysis method coupled with extraction to the organic phase and its comparison to known methods, *J. Pharm. Biomed. Anal.*, 2025, **255**, 116665, DOI: 10.1016/j.jpba.2025.116665.

49 J. A. Mitchell, P. Akarasereenont, C. Thiemermann, R. J. Flower and J. R. Vane, Selectivity of nonsteroidal antiinflammatory drugs as inhibitors of constitutive and inducible cyclooxygenase, *Proc. Natl. Acad. Sci. U. S. A.*, 1993, **90**, 11693–11697, DOI: 10.1073/pnas.90.24.11693.

50 N. H. Houngbedji, Š. Štěpánková, V. Pflégr, K. Svrčková, M. Švarcová, J. Vinšová and M. Krátký, Novel Inhibitors of Acetyl- and Butyrylcholinesterase Derived from Benzohydrazides: Synthesis, Evaluation and Docking Study, *Pharmaceuticals*, 2023, **16**, 172, DOI: 10.3390/ph16020172.

51 J. Rumpf, R. Burger and M. Schulze, Statistical evaluation of DPPH, ABTS, FRAP, and Folin-Ciocalteu assays to assess the antioxidant capacity of lignins, *Int. J. Biol. Macromol.*, 2023, **233**, 123470, DOI: 10.1016/j.ijbiomac.2023.123470.